An Improved Bio-Physical Parameterization for Radiant Heating in the Surface Ocean

Carson R. Witte[1], Ajit Subramaniam[1], and Christopher J. Zappa[1]

[1]Lamont-Doherty Earth Observatory, Columbia University

Corresponding author: Carson R. Witte (cwitte@ldeo.columbia.edu)

Key Points:

- Using empirical physical modeling tools, we develop a bio-physical radiant heating parameterization that remedies a gap in the literature.
- In-situ observations of the underwater and surface solar spectrum and the surface albedo are used to probe the parameterization's accuracy.
- The parameterization is applied in a first-of-its-kind case study of the sensitivity of diurnal warm layers to chlorophyll concentration.

Abstract

Solar heating of the upper ocean is a primary energy input to the ocean-atmosphere system, and the vertical heating profile is modified by the concentration of phytoplankton in the water, with consequences for sea surface temperature and upper ocean dynamics. Despite the development of increasingly complex modeling approaches for radiative transfer in the atmosphere and upper ocean, the simple parameterizations of radiant heating used in most ocean models are plagued by errors and inconsistencies. There remains a need for a parameterization that is reliable in the upper meters and contains an explicitly spectral dependence on the concentration of biogenic material, while maintaining the computational simplicity of the parameterizations currently in use. In this work, we assemble simple, observationally-validated physical modeling tools for the key controls on ocean radiant heating, and simplify them into a parameterization that fulfills this need. We then use observations from 64 spectroradiometer depth casts across 6 cruises, 13 surface hyperspectral radiometer deployments, and 2 UAV flights to probe the accuracy and uncertainty associated with the new parameterization. We conclude with a case study using the new parameterization to demonstrate the impact of chlorophyll concentration on the structure of diurnal warm layers, an investigation that was not possible to conduct accurately using previous parameterizations. The parameterization presented in this work equips researchers to better model global patterns of sea surface temperature, diurnal warming, and mixed-layer depths, without a prohibitive increase in complexity.

Plain Language Summary

Most of the sunlight that hits our planet is absorbed by the ocean as heat, and the vertical distribution of this heat influences the circulation patterns of the atmosphere and upper ocean. Phytoplankton in the ocean also absorb sunlight, preventing it from heating deeper water. It is important, therefore, for ocean models to have a realistic representation of the solar heating profile as a function of the phytoplankton concentration. However, there are issues with current parameterizations of solar heating in ocean models. To remedy this, we use intuitive physical modeling tools to develop a new parameterization that balances simplicity and accuracy and can be applied across all types of ocean modeling. We compare our parameterization to several types of direct measurements to better understand its accuracy and limitations. Finally, we conclude with a case study demonstrating the value of the new parameterization in an application that was previously not possible.

1 Introduction

Sunlight is the primary energy input to our planet, and with over 70% of the earth's surface covered by water, solar heating of the ocean plays a fundamental role in the behavior of the coupled ocean-atmosphere system at scales large and small. Though it is often conceptualized as a surface flux to the well-mixed upper layer of the ocean, some wavelengths of sunlight can penetrate quite deep before being completely absorbed as heat, and any light that penetrates deeper than the mixed layer will reinforce the stratification of the underlying pycnocline, effectively decoupling it from direct influence on the sea surface temperature (SST). The vertical distribution of solar heating is sensitive to the amount of absorptive material in the water, and in the open ocean where phytoplankton and their derivatives are the primary absorbing constituents ("case I waters"), the spectral absorption has been empirically shown to follow a robust power-law relationship to the chlorophyll concentration (Morel, 1988; Morel et al., 2007; Morel & Maritorena, 2001). Consequently, spatiotemporal variability of the phytoplankton system in the

surface ocean exerts a significant influence on SST, mixed-layer heat budgets, and upper ocean dynamics (Gildor et al., 2003; Iudicone et al., 2008; Kahru et al., 1993; Kantha & Clayson, 1994; Murtugudde et al., 2002; Ohlmann et al., 1998; Sathyendranath et al., 1991; Simpson & Dickey, 1981; Zaneveld et al., 1981). The formation and evolution of diurnal warm layers (DWLs), which can span broad areas of the tropical oceans, is especially sensitive to variability in the vertical distribution of solar heating (Bellenger & Duvel, 2009; Dickey & Simpson, 1983). At larger scales, phytoplankton-induced SST variability may modify the strength of the Hadley and Walker circulations (Gnanadesikan & Anderson, 2009), steer tropical cyclones away from the equator (Gnanadesikan et al., 2010), slow the meridional overturning circulation (Sweeney et al., 2005), and perhaps even play a role in Arctic Amplification (Hill, 2008). Meanwhile tantalizing evidence has been mounting for a possible coupling between phytoplankton and both the Madden-Julian Oscillation (MJO) and El Nino-Southern Oscillation (ENSO), in which wind bursts upwell nutrients and stimulate phytoplankton blooms, which subsequently trap solar radiation near the surface, increasing SST and thereby atmospheric convection during the quiescent phases of these oscillatory climate modes (Jin et al., 2013; Jochum et al., 2010; Lengaigne et al., 2007; Marzeion et al., 2005; Siegel et al., 1995; Strutton & Chavez, 2004).

The coupling between ocean physics and biology is an important piece of the climate system that has yet to be fully untangled. In one study coupling an ocean biogeochemical model to an ocean general circulation model, Manizza et al. (2005) found that modification of light penetration by phytoplankton biomass amplified the seasonal cycles of temperature, mixed layer depth, and sea ice cover by 10%, and these physical changes caused increases in phytoplankton biomass, a positive feedback that further amplified the physical perturbations. Another study by Wetzel et al. (2006) added a marine biogeochemical model to a fully coupled atmosphere-ocean climate model, and in addition to observing similar amplifications in the magnitude of the seasonal cycle, the timing of the seasons became more realistic, with spring starting two weeks earlier. These coupled experiments rely on formulations for the physics of solar absorption that are expressed as a function of chlorophyll concentration, as this is a primary output of biogeochemical models. Modern remote-sensing tools enable the retrieval of attenuation coefficient estimates at specific wavelengths from satellites, and this has led some investigators to suggest that the direct observations of the optical properties should be used in physical modeling (e.g. Liu et al., 2020). While there are good reasons for this approach and undoubtedly research contexts in which it is the smart choice, it introduces significant complexity and largely precludes the possibility of coupling the physics to the biology through the shared variable of chlorophyll concentration. Thus we emphasize the continued need for a simple, chlorophyll-dependent parameterization of radiant heating in the modern oceanographer's toolkit.

Despite an abundance of evidence as to the importance of (primarily biogenic) in-water absorbing constituents to the mixed-layer heat budget and SST, the extensive literature exploring this bio-physical interaction has been riddled with errors, due at least in part to the inter-disciplinary nature of bio-physical reseach. We present here a brief history of the development of expressions for radiant heating in the surface ocean, and a discussion of their mis-application in various studies.

1.1 Foundational Work

Early research represented the underwater irradiance profile as a single exponential (e.g. Denman, 1973). While this is physically valid for a given wavelength, it is problematic when

applied to the broadband solar irradiance due to spectral variability in the exponential decay rates, which span many orders of magnitude across the wavelengths in the solar spectrum. Kraus (1972) is generally credited as the first to suggest using a sum of two exponentials. Paulson & Simpson (1977) fit a double-exponential form to Jerlov (1968, 1976)'s data for different optical water types, and this became the standard parameterization used in many mixed-layer models even to this day (e.g. Price et al., 1986). While the two exponentials are nominally split somewhere around the edge of the visible domain, the split is not explicitly spectral and the exponentials are simply tuned to best fit the available data. Zaneveld & Spinrad (1980) employed an alternative fitting approach to the same underlying Jerlov data, using an arc-tangent curve to better represent the rapid extinction of irradiance in the upper 10 meters. While these parameterizations were an important step along the journey, the approach of choosing between qualitative optical water types is outdated, thus we suggest that parameterizations based on Jerlov data should not be in use today. Several other parameterizations were also developed in the early 1980s to pursue specific physical research questions. Paulson & Simpson (1981) fit 9 explicitly spectral bands originally calculated by Schmidt (1908) and catalogued in Defant (1961) for the purpose of calculating solar absorption across the ocean skin – this parameterization was employed in early iterations of the COARE cool-skin correction (Fairall, Bradley, Godfrey, et al., 1996), but was shown to be inaccurate and modified for newer versions to better fit available data (Wick et al., 2005). Given that it is built on a very small sample of laboratory data acquired at the turn of last century using measurement techniques that have since been improved upon many times over, it too should not be used. Finally, Soloviev (1982) performed a three-exponential fit to a combination of Jerlov data and a near-surface underwater irradiance profile provided by Ivanoff (1977) to estimate a parameterization that remains in use in modern warm layer studies (Fairall, Bradley, Godfrey, et al., 1996).

As the importance of biological agents in modifying visible-wavelength attenuation became evident, chlorophyll-dependent spectral parameterizations were developed for the visible domain as an improvement over Jerlov's qualitative water types (e.g. Siegel & Dickey, 1987; Smith & Baker, 1978). This culminated in the work of Morel (1988), who combined 176 spectral downwelling irradiance measurements from 12 cruises and fitted a power-law relationship to predict spectral attenuation from chlorophyll concentration in 5nm bins across the 400-700nm visible domain. Morel & Antoine (1994) then expanded the relationship to cover the full solar spectrum for use in radiant heating studies, and this has served as the basis for most subsequent chlorophyll-dependent parameterizations. However, the underlying work of Morel (1988) has since been updated several times to incorporate more field data and better measurements of the water's contribution to the attenuation (Morel et al., 2007; Morel & Maritorena, 2001).

With the development of increasingly powerful radiative transfer models came the opportunity to simulate a wide variety of conditions and develop parameterizations from model outputs. Ohlmann & Siegel (2000) used the HYDROLIGHT model to generate a full suite of irradiance profiles for a wide range of chlorophyll concentrations, solar zenith angles, and cloud indices, and then fit their results to a 4-exponential form without explicit spectral partitions. In a follow-up paper, Ohlmann (2003) provides a simplification of the model dependent only on chlorophyll concentration for use in climate models, at the cost of accuracy in the upper meters. And finally, Lee et al. (2005) tried to improve upon this approach by developing an explicitly spectral 2-band parameterization using the HYDROLIGHT model, this time as a function of satellite-observable properties (absorption and backscatter at 490nm).

1.2 Issues in the Literature

Application of the parameterizations discussed in Section 1.1 to various modeling efforts has been subject to a number of errors. These errors do not necessarily call into question the fundamental findings of the studies, but they have been propagated through multiple publications to the point that they are deeply rooted in the literature, introducing unnecessary inaccuracy into our research on bio-optical phenomena.

One pervasive issue infecting decades of work is the misinterpretation of the two exponential bands presented in Paulson & Simpson (1977). These exponential functions were developed by fitting underwater profiles of broadband irradiance in different depth segments, with one exponential fit to the irradiance profile below 10m, and the other fit to the irradiance profile in the top 6m. The fractions of incident irradiance assigned to the two bands just reflect the best fit to the data, not a division of the solar spectrum at a particular wavelength. Yet Manizza et al., (2005) mistook the partitioning between Paulson & Simpson (1977)'s two exponential bands to be an explicitly spectral split located at 700nm, consequently assigning 42% of the incident irradiance to the visible (400:700nm) waveband in their spectral model. There is an abundance of observational evidence that the visible fraction of incident irradiance is approximately 45-47% under clear skies (Britton & Dodd, 1976; Frouin et al., 1989; Goldberg & Klein, 1977; Howell et al., 1983; Ivanoff, 1977; Kirk, 1994; Kvifte et al., 1983; McCree, 1966; Moon, 1940; Papaioannou et al., 1993; Rao, 1984; Rodskjer, 1983; Strutton & Chavez, 2004; Weiss & Norman, 1985; Yocum et al., 1964), and increases up to ~60% with increasing cloud cover (Blackburn & Proctor, 1983; Frouin et al., 1989; Nann & Riordan, 1991; Siegel et al., 1999; Tanre et al., 1979, and see Section 4 for further observational validation). It is fortuitous that the 42% partition presented in Paulson & Simpson (1977) for Jerlov Type I waters is reasonably close to the spectral estimate of 45-47% (had a different decision been made as to the qualitative water type, the partitioning would have been considerably less accurate). Manizza et al. (2005) then made the unsubstantiated assumption that the visible-wavelength band could be further split at 530nm with 50% of the visible irradiance assigned to each band – as it turns out, the modeling tools we introduce in Section 2 suggest that a 45/55% split would be more appropriate.

This unnecessarily erroneous setup has since been propagated into major earth system models, including the American GFDL-ESM4.1 (Stock et al., 2020), Australian ACCESS-OM2 (Kiss et al., 2020), and Chinese BCC-CSM2 (Wu et al., 2021). It also appears regularly in bespoke modeling efforts to elicit key features of bio-physical interactions (e.g. Gnanadesikan & Anderson, 2009; Holmes et al., 2019; Kim et al., 2015; Lengaigne et al., 2007; Lim et al., 2019; Moeller et al., 2019; Twelves et al., 2021). While we anticipate that the broad conclusions arrived at in these studies are unlikely to be significantly altered by this error, there is simply no reason for it to remain an issue in ocean modeling going forward, and the parameterization developed in this work offers a straightforward replacement.

In addition to the misuse of Paulson & Simpson (1977) for spectral partitioning, there are other cases in the literature of the wrong parameterization being selected for the task at hand. For example, Prytherch et al. (2013) updated the Diurnal Warm Layer (DWL) model of Fairall et al. (1996) to use the chlorophyll-dependent parameterization of Ohlmann (2003) rather than the default profile from Soloviev (1982). Yet Ohlmann (2003) explicitly states that "the parameterization is not valid for depths shallower than 2m," making it a terrible choice for DWL modeling. Unsurprisingly, Prytherch et al. (2013) report that accurate representation of solar absorption still appears to be a primary confounding factor in modeling DWLs.

Similarly, Gentemann et al. (2009) set out to improve upon the DWL model of Fairall et al. (1996), and one of the key changes they chose to make was using the 9-band spectral parameterization of Paulson & Simpson (1981), the reason given being that it displays higher absorption near the surface compared to that of Soloviev (1982). As discussed in Section 1.1, this parameterization is based on a small dataset acquired using outdated laboratory practices >100 years ago, and there is no justifiable reason for its continued use when far better studies have been conducted in the interim. In the end, Gentemann et al. (2009) had to multiply the solar absorption profile by 1.2 in order to get their model to agree well with observations. The parameterization developed in this work provides a much better option for future DWL modeling efforts.

1.3 Purpose of This Work

Thus far we have discussed how the simple parameterizations of upper ocean radiant heating used in most modern models are plagued by errors and inconsistencies. Indeed, there is no parameterization in use that fulfills these criteria:

1) computationally efficient enough for large models
2) accurate within the upper few meters of the ocean
3) accounts for the effect of biogenic substances
4) explicitly spectral in the photosynthetically active (400:700nm) domain

In this work, we develop a parameterization that fulfills the above criteria. We begin by assembling simple, observationally-validated physical modeling tools for the key controls on upper ocean radiant heating, creating an intuitive spectral model. We simplify the spectral model to a useable parameterization that can be directly implemented in existing ocean models, comparing our results to prior parameterizations. We then use observational datasets to inform our understanding of the uncertainties associated with this parameterization, and conclude with a case study demonstrating the impact of chlorophyll concentration on the formation and evolution of diurnal warm layers.

2 The Full Spectral Model

The purpose of this section is to develop a spectral model for ocean radiant heating that is conceptually and computationally accessible, and requires a minimum of input parameters. While sophisticated radiative transfer modeling tools (see e.g. Mobley, 1994; Ricchiazzi et al., 1998 as a starting point) might enable a more complete description of the process, their complexity presents an unnecessary impediment to our ultimate objective of a simple and reliable radiant heating parameterization. By assembling pre-existing, observationally validated models for the solar spectrum at the ocean surface, the broadband albedo, and the spectral underwater attenuation, we create a radiant heating model that is both accurate and accessible, needing as inputs only the downwelling broadband irradiance, the chlorophyll concentration, and the time and location on the earth. The spectral model, summarized graphically in Figure 1 and as a flow-chart in Figure 2, is both a step towards a useful parameterization, and a valuable tool to help build intuition for the interaction between sunlight and the atmosphere-ocean system.

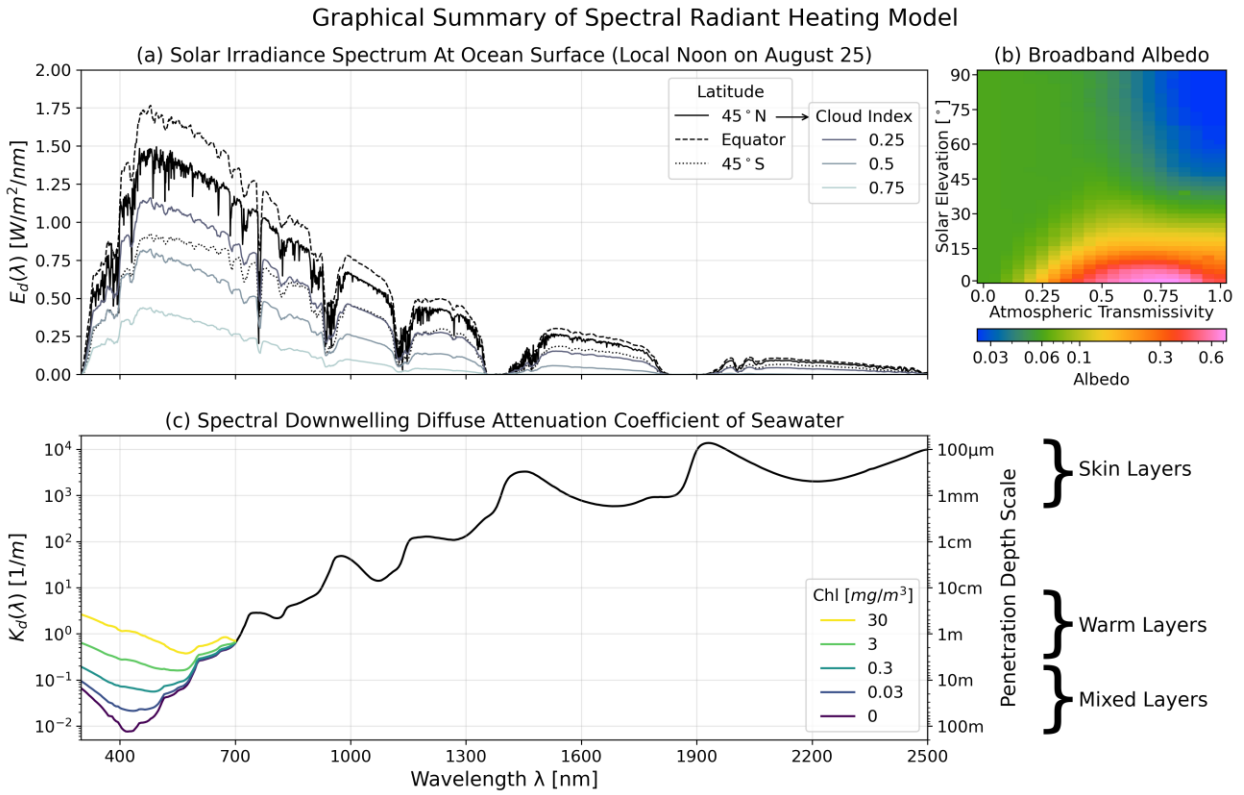

Figure 1: Graphical depiction of spectral model components. (a) Clear-sky spectra from Diffey (2015) at 3 latitudes for an example date & time, differentiated by line style. For the 45N latitude, the modification of the spectrum by the cloud index model of Siegel (1999) is shown with color, demonstrating the preferential transmission of shorter wavelengths through clouds. (b) Broadband albedo from Payne (1972) as a function of atmospheric transmissivity and solar elevation, shown on a logarithmic color scale. (c) Diffuse attenuation coefficients at each wavelength in the solar spectrum, with chlorophyll-dependence in the UV and visible from Morel et al. (2007), and infrared coefficients from Bertie & Lan (1996).

2.1 Clear-Sky Solar Irradiance Spectrum

To predict the solar irradiance spectrum at the ocean surface under clear skies, we employ the model of Diffey (2015), who deliberately set out to "develop a model that is as simple as it can be commensurate with delivering results of adequate accuracy." By starting from a reference spectrum and accounting for solar angle, direct and diffuse radiation, Rayleigh scattering, aerosol scattering and absorption, and ozone absorption, they demonstrate good agreement with both observations and radiative transfer modeling using nothing more complex than an Excel spreadsheet with time and position as inputs. The Excel sheet was carefully translated into Python for use in this study.

2.2 Spectral Influence of Clouds

Having predicted the solar irradiance under a clear sky, we calculate the "Cloud Index" *CI* of the sky in terms of the ratio between observed and predicted broadband irradiances:

$$CI = 1 - \frac{SW_{observed}}{SW_{clear-sky}}$$

where $SW_{clear-sky}$ comes from integrating the clear-sky spectrum predicted in Section 2.1. We then employ the empirical model of Siegel et al. (1999) to relate our broadband Cloud Index to a wavelength-specific cloud index, scaling each wavelength in the clear-sky spectrum by a different amount to accurately reflect the changes in spectral composition caused by clouds (namely, preferential transmission of shorter wavelengths). This leaves us with a final estimate for the solar spectrum at the ocean surface, which integrates to $SW_{observed}$.

2.3 Albedo

The albedo of the sea surface does vary with wavelength, with shorter wavelengths tending to have a slightly higher albedo than red and infrared (Ohlmann et al., 2000, see their Figure 12). However, the magnitude of spectral variability and the absolute magnitude of the albedo are both so small that the spectral effects are second- or even third-order from a radiant heating perspective, and thus we do not account for them in this model. Rather, we use the empirical model of Payne (1972), which predicts a broadband albedo as a function of the sun angle and the transmissivity of the atmosphere (equivalent to one minus the Cloud Index). This lookup table was developed from four months of observations at the mouth of Buzzards Bay, Massachussets, and validated against radiative transfer modeling by Ohlmann et al. (2000). The albedo may also display a small wind speed dependence at low sun angles (Katsaros et al., 1985; Payne, 1972) but low sun angles generally correspond to low absolute irradiances and are therefore of minor concern in the context of radiant heating studies outside of the high latitudes.

2.4 Underwater Attenuation

To account for the effect of biogenic substances in the water on the attenuation of UV and visible light, we use the bio-optical parameterization originally published by Morel (1988) and most recently updated in Morel et al. (2007). The parameterization rests on the assumption that at each wavelength, the spectral attenuation coefficient K_d can be decomposed into two additive parts:

$$K_d = K_w + K_{bio}$$

where K_w is the attenuation due to the water itself, and K_{bio} is the combined attenuation due to all biogenic substances in the water (including algal cells, detritus, colored dissolved organic matter, and other associated nonalgal organisms). The "bio-optical assumption" states that the total attenuating effect of all biogenic substances in the water co-varies with chlorophyll in a consistent way; the Morel publications have demonstrated that this assumption is reasonable in open ocean (or "case I") waters, with K_{bio} following a power-law relationship to chlorophyll concentration:

$$K_{bio}(Chl, \lambda) = \chi(\lambda)[Chl]^{e(\lambda)}$$

where $\chi(\lambda)$ and $e(\lambda)$ are empirical parameters determined by a linear fit to $[Chl]$ vs. K_{bio} observations in natural-log space at each wavelength λ. Morel et al. (2007) only published their parameterization down to 350nm, so we follow the approach of Morel & Antoine (1994) in extrapolating the parameterization between 300:350nm. For $\lambda >$700nm, the attenuation due to the water itself is so strong that biogenic substances have negligible influence. We therefore use the "gold standard" laboratory data from Bertie & Lan (1996) for attenuation coefficients in the infrared.

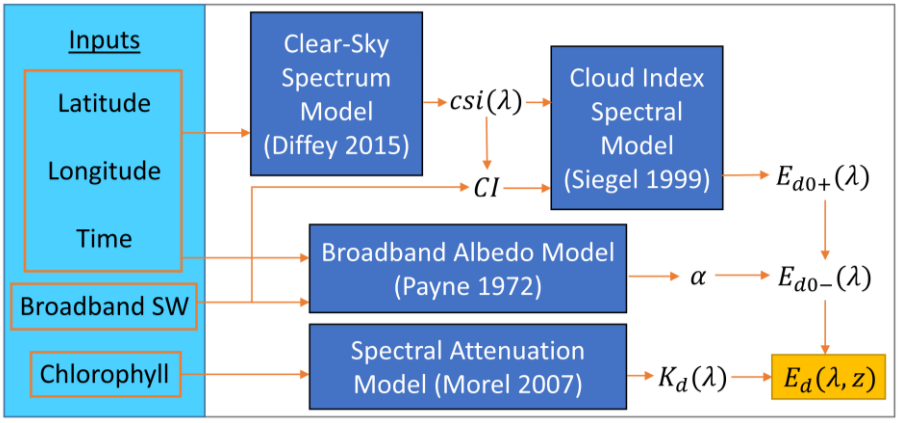

Figure 2: Flowchart demonstrating how the modeling tools depicted in Figure 1 and described in Section 2 can be combined for use as a spectral radiant heating model.

3 The Final Parameterization

Despite its simplicity, the spectral model derived in Section 2 is far too complex to be reasonably integrated into most ocean modeling. From large-scale coupled climate models to 1-D mixed-layer models, most ocean models represent the underwater irradiance profile as the sum of just a few exponentials. Our purpose in this section is therefore to simplify our spectral model to just a few wavelength bands while balancing simplicity and accuracy. To do this, we first simplify the underwater attenuation coefficients, and then determine how to partition the incident irradiance between the resulting spectral bands.

3.1 Simplifying the Model to a Useful Parameterization

In order to simplify the parameters of the bio-optical fits and preserve the chlorophyll-dependence of the model in the UV and visible, we took logarithmic averages of each parameter (K_w, χ, and e) within a specified wavelength band. Within the UV band from 300:400nm, we improved the agreement with the spectral model by weighting the average using a typical irradiance spectrum, which helps account for how little light there is in the 300:350nm range compared to the 350:400nm range. For the Visible (PAR) wavelengths from 400:700nm, we sought to divide the spectrum into the minimum number of bands necessary to accurately reproduce the fully spectral output. While just two visible-wavelength bands have been employed in the past (e.g. Manizza et al., 2005), we found that two bands introduced too much vertical variability in the profiles compared to the full spectral model regardless of the location of the split, while three bands (with splits at 510nm and 600nm) reproduce the full spectral model almost perfectly. Parameters for the four resulting wavelength bands are given in Table 1.

The infrared wavelengths present a different challenge. While there is no chlorophyll-dependence that must be preserved through the simplification, the attenuation coefficients span so many orders of magnitude between 700:2500nm that the resulting irradiance profile in the upper meter of the ocean decreases much more rapidly than a simple exponential. In trying to fit the profile as a sum of exponentials, we found that we needed >10 exponential bands to reasonably approximate the profile, which presents a good deal of computational complexity compared to the parameterizations we intend to replace. Rather than accept a poor fit with fewer

exponentials, we follow the pioneering example of Zaneveld & Spinrad (1980) in using an arctangent curve to approximate the rapid decrease near the surface. We fit modeled profiles generated from a wide variety of input conditions to the form:

$$e^{-C_1 z}[1 - C_2 \arctan(C_3 + C_4 z)]$$

and found the fit constants C_{1-4} (given in Table 1) that best reproduce the spectral model output.

Having defined five wavelength bands and produced reliable descriptions of each band's decay with depth, we must determine what fraction of the incident broadband irradiance should be assigned to each band. In order to do so, we initialized the spectral model with a range of input conditions that span the parameter spaces for sun angle, cloud index, and chlorophyll, and found the constant partitions between the five simplified bands that minimized the absolute difference between the spectral model outputs and the five-band parameterization. The resulting partitions are 6% UV, 49% infrared, and 45% visible (subdivided into 17% blue, 14% yellow, and 14% red). These correspond to a cloud index of ~0.2 in the spectral model.

Finally, the albedo is generally such a small percentage of the incident irradiance that radiant heating parameterizations have historically treated it as a constant. As can be seen in Figure 1b, the Payne (1972) model yields an albedo of ~0.055 across the majority of relevant conditions, with slightly lower albedos under very clear skies, and significantly higher albedos in conditions of very low sun angles. Because low sun angles correspond to low absolute irradiances, neglecting the variability in albedo yields very small absolute errors. We therefore follow the established literature (e.g. Fairall, Bradley, Rogers, et al., 1996) in setting a constant albedo of 0.055 for our parameterization. The final parameterization is summarized in Table 1.

Table 1: The Final Radiant Heating Parameterization.

Waveband [nm]	**Partition (F)**	**Transmission Profile** (multiply by 0.945*SW)	**Parameters**	
300:400 (UV)	0.06	$Fe^{-K_d z}$ where $K_d = K_w + \chi[Chl]^e$	$K_w = 0.0218$	
			$\chi = 0.1758$	
			$e = 0.6541$	
400:510 (Blue)	0.17	$Fe^{-K_d z}$ where $K_d = K_w + \chi[Chl]^e$	$K_w = 0.0119$	
			$\chi = 0.1048$	
			$e = 0.6330$	
510:600 (Yellow)	0.14	$Fe^{-K_d z}$ where $K_d = K_w + \chi[Chl]^e$	$K_w = 0.0665$	
			$\chi = 0.0582$	
			$e = 0.5342$	
600:700 (Red)	0.14	$Fe^{-K_d z}$ where $K_d = K_w + \chi[Chl]^e$	$K_w = 0.3608$	
			$\chi = 0.0585$	
			$e = 0.4723$	
700:2500 (IR)	0.49	$Fe^{-C_1 z}(1 - C_2 \arctan(C_3 + C_4 z))$	$C_1 = 1.87$	$C_2 = 0.47$
			$C_3 = 0.66$	$C_4 = 30$

3.2 Comparison to Existing Parameterizations

Figure 3 provides a revealing comparison between the new parameterization and several existing parameterizations, in terms of both the irradiance and heating profiles, in both linear and logarithmic depth-space. The parameterization aligns well with the more complex formulation of Ohlmann & Siegel (2000), particularly at high and moderate chlorophyll concentrations. The divergence at the lowest chlorophyll concentration is expected, due to our implementation of a more recent iteration of the bio-optical relationship, which is based on the significantly lower (and more accurate) values for the absorption of pure water from Pope & Fry (1997) as implemented in Morel et al. (2007), rather than the Smith & Baker (1981) pure-water spectrum implemented in Morel (1988) and used by Ohlmann & Siegel (2000). In fact, further revisions to the pure-seawater absorption (Lee et al., 2015; Mason et al., 2016) and scattering (Zhang et al., 2009) spectra have been published since Morel et al. (2007), with even lower values in the blue wavelengths, but the changes are small enough that they do not yield appreciable differences when integrated for radiant heating calculations. Among the classical parameterizations without Chlorophyll-dependence, we observe the best agreement with Soloviev (1982), particularly near the surface. This reveals why efforts to improve DWL modeling have struggled when switching away from Soloviev (1982), as other options (such as the Paulson & Simpson (1977) & (1981) parameterizations also plotted in Figure 3) perform markedly worse in the upper meters. Indeed, any parameterization built on Paulson & Simpson (1977), including Manizza et al. (2005), will likely perform equally poorly near the surface.

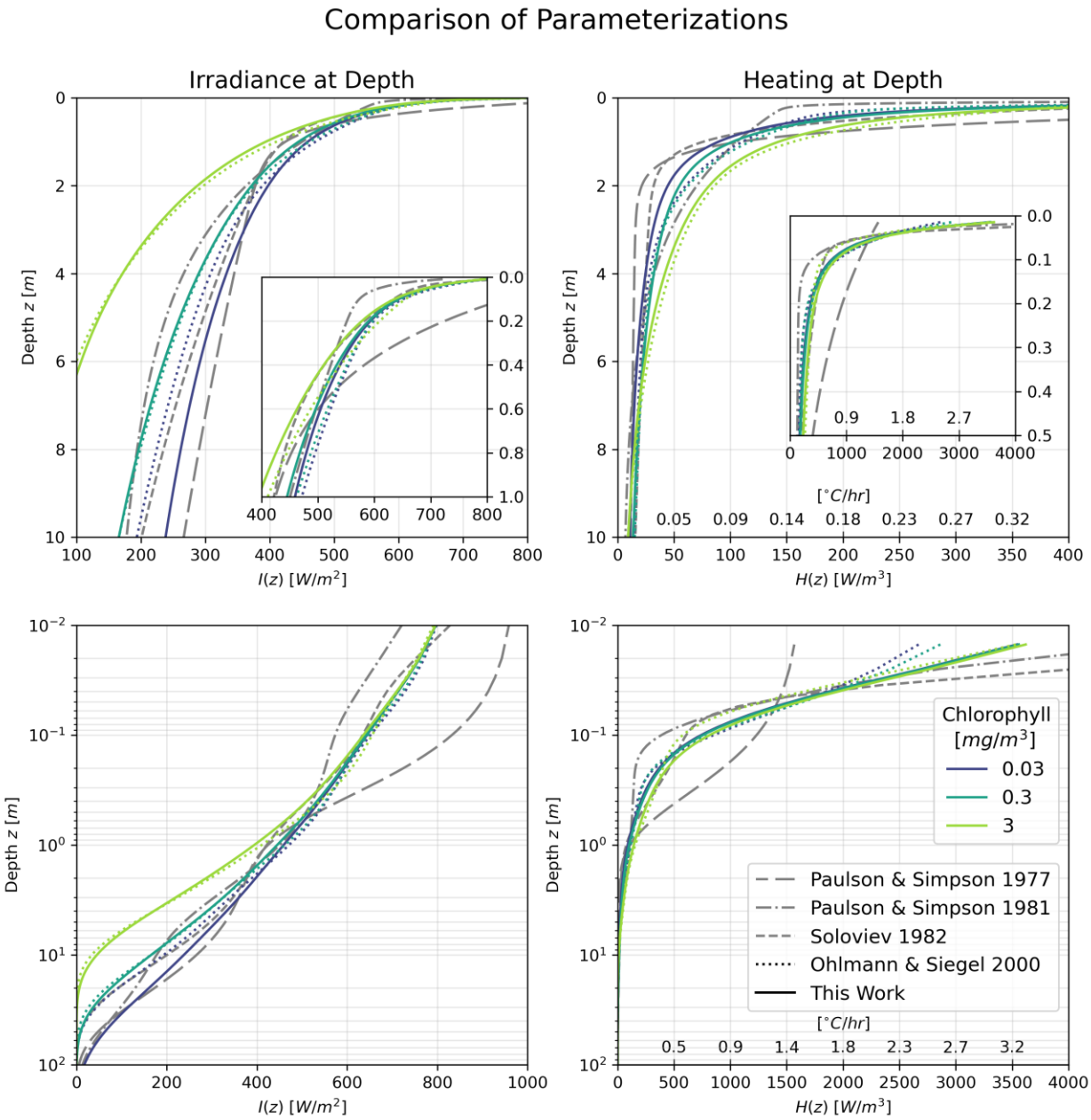

Figure 3: Comparison of the parameterization developed in this work to several parameterizations in the literature. The left panels show profiles of irradiance with both linear (top) and logarithmic (bottom) depth scales, while the right panels show the resulting profiles of heating. Ohlmann & Siegel 2000 is plotted in dotted lines colored by chlorophyll concentration, for comparison with our new parameterization plotted in solid lines colored by chlorophyll concentration. The classical parameterizations that do not include chlorophyll dependence are plotted in grey, distinguished by line style.

4 Uncertainty & Observations

The simplest approach to estimating the uncertainty associated with our parameterization is to compare it to the outputs of the full spectral model, initialized across a broad range of input conditions. The differences – plotted against depth in Figure 4 – portray an envelope of potential uncertainty, and the color gradient reveals a pronounced Cloud Index dependence, with positive differences at low Cloud Indices and negative differences at high Cloud Indices. Line styles in

Figure 4 represent different input chlorophyll concentrations; at a given Cloud Index, lower chlorophyll concentrations generally correspond to higher absolute differences at depth, simply because more light is able to penetrate deeper. However, the parameterization and model agree well at a Cloud Index of 0.2, and changes in chlorophyll concentration at this Cloud Index yield no change in the difference between model and parameterization. This implies that the chlorophyll-dependence is well captured by the parameterization, while the biggest factor that is neglected in the parameterization is the spectral influence of clouds. The comparisons in Figure 4 would suggest an uncertainty estimate of ±30 W/m^2 in the upper meters. However, although the spectral model is built on observationally-validated tools, we must be cautious in interpreting it as an absolutely true representation of real-world behavior. We therefore turn to several types of in-situ observations to shed further light on the validity of both the parameterization and the spectral model.

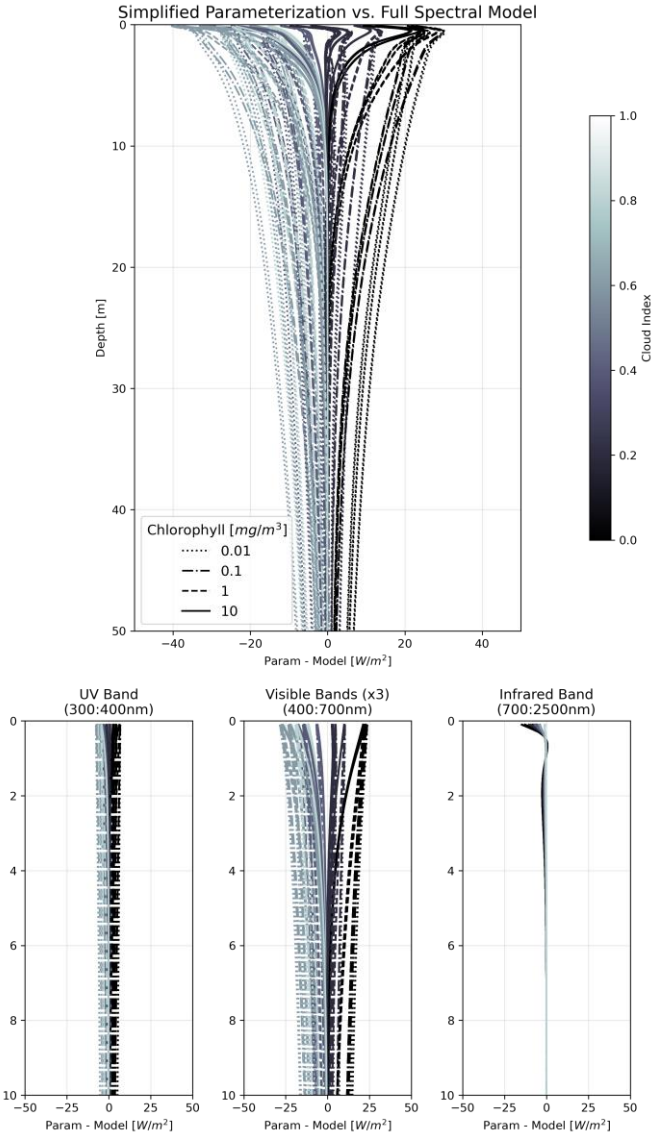

Figure 4: Comparison of the simplified parameterization to the full spectral model in the upper 50m across the parameter space of input conditions. The colors reveal that the differences are largely due to the inclusion/exclusion of cloud effects. The lower panels

show the upper 10m split out by wavelength region, revealing the visible region to be the dominant source of variability.

4.1 Profiling Multi-Spectral Radiometer Observations

We can test the visible-wavelength portions of both the full model and simplified parameterization using a dataset of 140 profiling spectroradiometer depth casts (Satlantic Profiler II equipped with 2 OCI 507 and 2 OCR 507 radiometers for a total of 14 wavelength channels spanning 380-705nm) with coincident pyranometer and chlorophyll measurements, collected on 2 cruises in the tropical Atlantic (September 2015 and August 2016 onboard R/V Meteor), 3 cruises in the Gulf of Mexico (June 2015, August 2018 and July 2019 onboard R/V Endeavour), and one cruise in the Tropical Pacific (November 2019 onboard R/V Falkor). The casts were carefully quality-controlled, and only included in the final dataset if the standard deviation of pyranometer measurements during the cast was less than 50 W/m^2 (because a single pyranometer measurement and resulting Cloud Index value must be assigned to each cast), resulting in a final dataset of 64 casts. Each spectrally integrated visible irradiance profile observation was then compared to the profiles predicted by both the model and the parameterization. Figure 5 shows the results of the comparison, with the surprising result that the simplified parameterization appears to perform better than the full model at reproducing these observations, particularly at shallow depths. The spread in differences suggests the parameterization is reliable to within about ±25 W/m^2 in the visible wavelengths, which seem to be the main spectral region of uncertainty based on Figure 4. Given that Cloud Index dependence is the primary difference between parameterization and spectral model, the superior performance of the parameterization suggests the Cloud Index dependence of the spectral model may be too strong. We will further investigate this possibility using a dataset of surface hyperspectral radiometer observations.

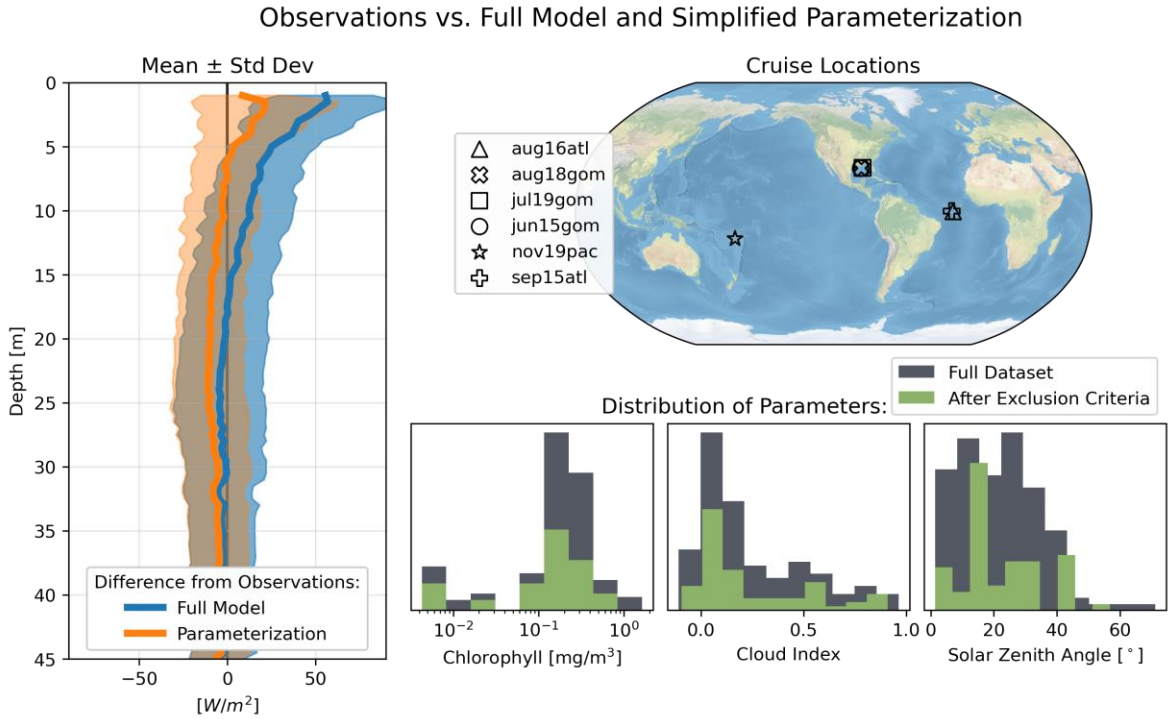

Figure 5: Comparison of integrated visible-wavelength irradiance profiles from 64 multi-spectral depth casts across 6 cruises to both the spectral model (blue) and simplified parameterization (orange). The map shows the locations of the cruises, and

the histograms show the distribution of model input parameters demonstrating the range of conditions sampled.

4.2 Surface Hyperspectral Radiometer Observations

While onboard R/V Falkor in the Tropical Pacific near Fiji in November 2019, a floating hyperspectral radiometer (Seabird HyperOCR) was deployed behind the ship for 30 minutes near solar noon on 13 separate days to capture the downwelling spectrum in the 350-800nm range at 3.3nm resolution. These observations can be used to test the model predictions for partitioning of the three visible wavelength bands as a function of Cloud Index. Because the pyranometer (Kipp & Zonen CMP22) mounted on the ship's mast – which is used to calculate the Cloud Index – was several hundred meters away from the floating radiometer, there was a temporal lag in sky conditions that is particularly evident on days with variable cloudiness, which are the most important days for filling out the Cloud Index parameter space. We therefore aligned the radiometer observations with the appropriate Cloud Index estimates by performing a lag correlation between the pyranometer and the (spectrally integrated) radiometer, with the resulting lags ranging between 19 and 72 seconds depending on the wind speed and direction. Figure 6 presents a comparison of observations and model output as a function of Cloud Index – note the y-axes are given as fractions of the visible irradiance rather than total solar irradiance, as the observations only span this range completely. Although the model generally predicts close to the right partitions, the observations display minimal variation in the Cloud Index range of 0.0–0.2, supporting the hypothesis that the model is over-sensitive to Cloud Index, particularly in conditions of relatively few clouds.

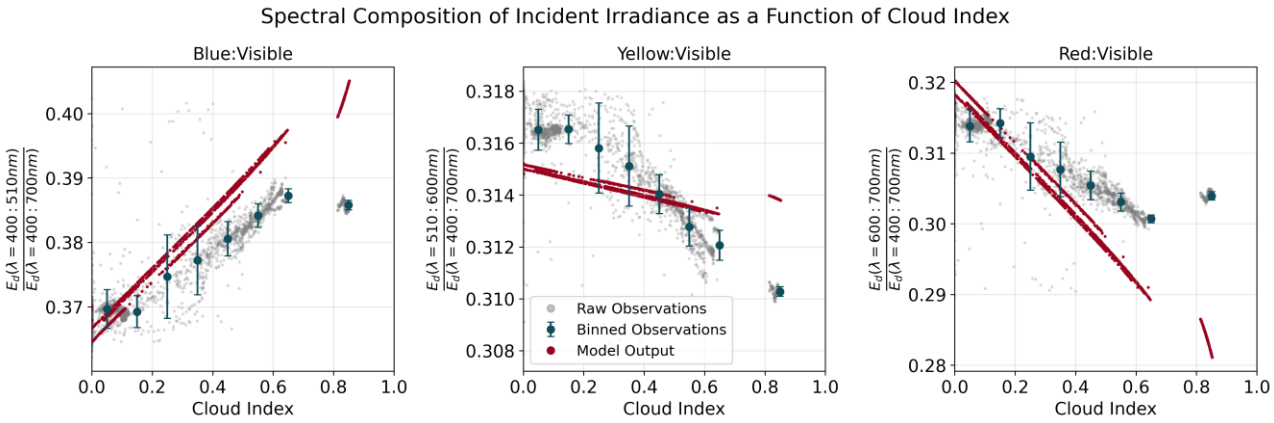

Figure 6: Partitioning of the three visible-wavelength bands defined in our parameterization as a function of Cloud Index. Floating hyperspectral radiometer observations are plotted in light grey, and binned by cloud index in blue. Model outputs are plotted in red.

4.3 UAV Albedo Observations

While a constant albedo was chosen for simplicity in the final parameterization, the Payne (1972) model displays albedos as high as 50% or more in low sun-angle conditions. For high-latitude applications, therefore, a variable albedo will likely be required. For this reason, we wish to interrogate the accuracy of the Payne (1972) model to determine its suitability for future use. Two Uncrewed Aerial Vehicle (UAV) flights were performed during the same 2019 R/V

Falkor cruise with a payload of matched up- and down-looking Hukseflux SR-03 Pyranometers. The downwelling irradiance measurements were corrected for platform motion following the procedure outlined in Reineman et al. (2013; see also Equation 5.1 in Bannehr & Glover, 1991) with a first-order Butterworth low-pass filter cutoff at 1/6 Hz. After correction, the dataset was subset to reject all points with roll or pitch values more than 1 degree from neutral, and then composited into 20-minute averages. Figure 7 shows the albedo observations from both flights compared to the Payne (1972) model (with model input parameters plotted in the lower panels). The observations and model output evolve similarly in time, but the observations are systematically lower than the model output by about 15% on average. This is unsurprising given that the Payne (1972) model is built on observations at the mouth of Buzzard's Bay, Massachussets, a turbid coastal environment that does not provide a generalizable analog to open ocean conditions. However, it is encouraging that the temporal evolution of the model follows the observations reasonably well, suggesting that the input parameters of solar elevation and atmospheric transmissivity have been properly identified as the primary controls on albedo variability. More observations of this kind are needed in open-ocean and high-latitude environments to build a more robust version of this simple and potentially very powerful modeling approach. Meanwhile, for studies employing a constant albedo, the limited observations we have thus far suggest that ~0.045 (15% lower than the current value) might be a better choice; however, more observations are needed before we advocate for implementing such a change.

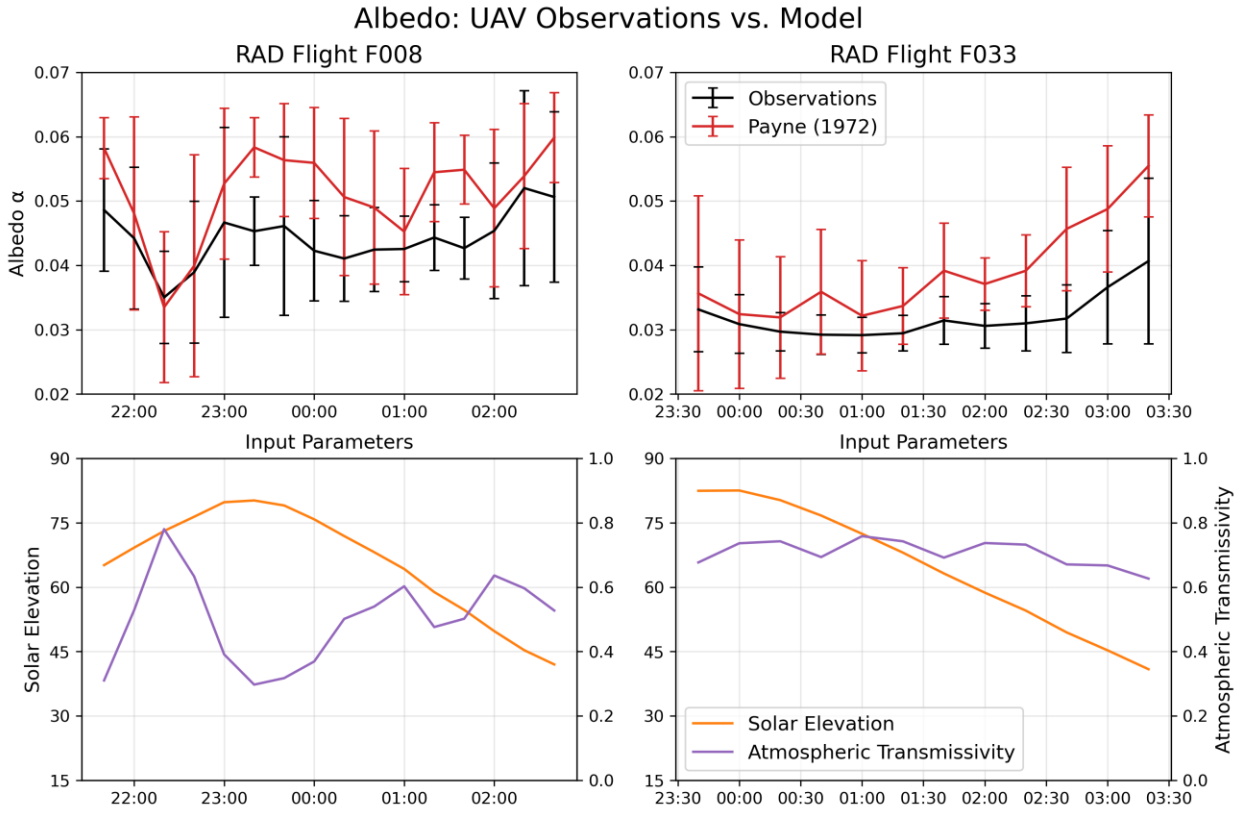

Figure 7: Albedo as measured directly during two UAV flights (black), compared to output of the Payne (1972) empirical model (red), with the input parameters for the model plotted in the lower panels.

5 Case Study: Sensitivity of Diurnal Warm Layers to Chlorophyll Concentration

The accuracy of our new parameterization near the surface presents an unprecedented opportunity to investigate the sensitivity of DWL formation to chlorophyll concentration. When the COARE3.5 model is forced with shipboard observations from the 2019 R/V Falkor cruise (referenced in previous sections), it predicts a DWL nearly every day. We therefore modified the COARE3.5 model to use the new parameterization, and ran multiple iterations of the model fed with different chlorophyll concentrations, with all other forcing taken from the shipboard observations and consistent between runs. The results, shown in Figure 8, demonstrate the impact that variations in chlorophyll can have on the magnitude and depth of DWLs. Under the same forcing conditions, the range of chlorophyll concentrations likely to be found in the open ocean can modify the strength of the DWL temperature gradient by several tenths of a degree, with higher chlorophyll leading to warmer layers, but significant variability between days (due primarily to the sensitivity of the DWL to wind forcing). Similarly, differences in chlorophyll can lead to changes in the depth of the warm layer of several meters, with higher chlorophyll corresponding to shallower layers. This is a generally intuitive result that more absorbing material in the water should lead to warmer and shallower DWLs as more radiant heating is trapped closer to the surface. These high-chlorophyll warm layers simultaneously have stronger static stability and larger air-sea temperature differences, with the consequence that more of their heat will be returned to the atmosphere via turbulent fluxes. This provides a clear mechanism by which the chlorophyll concentration could modulate the strength of atmospheric convection.

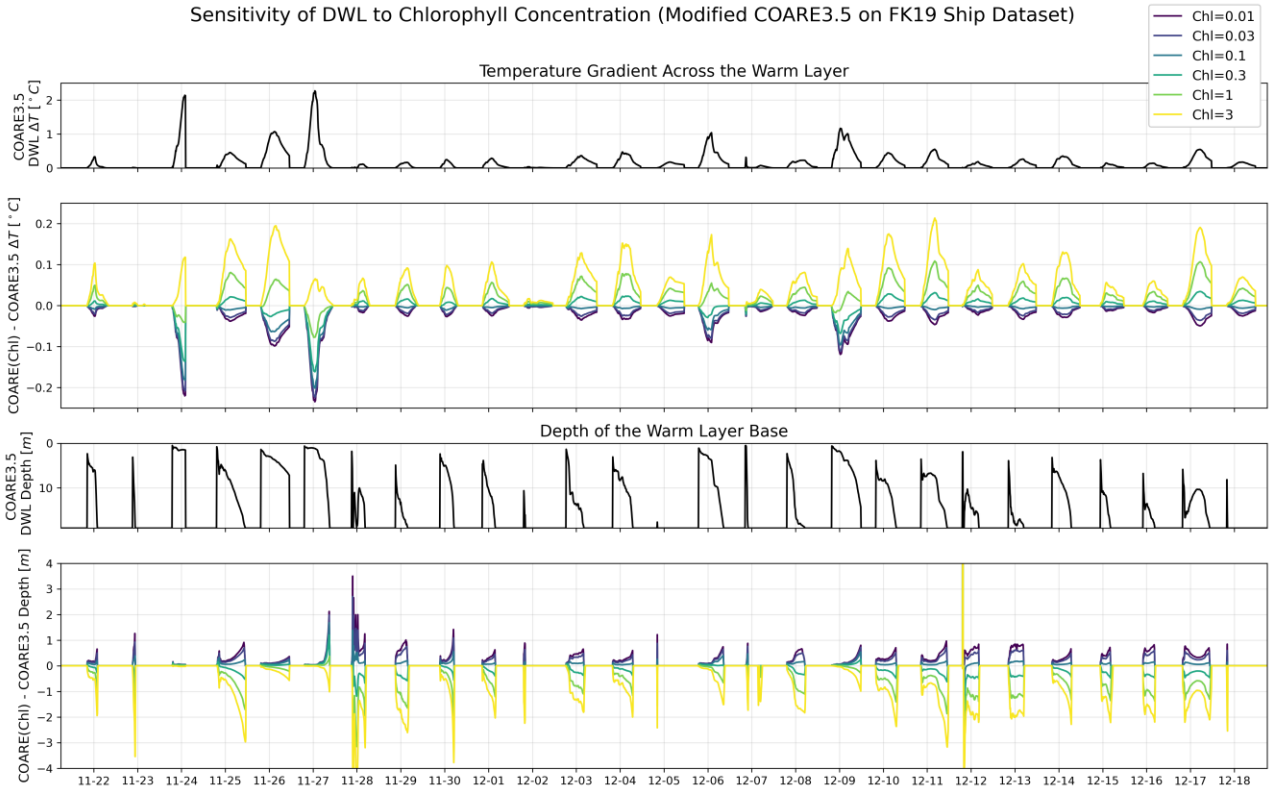

Figure 8: Results of modifying the COARE3.5 diurnal warm layer model to use our new parameterization, and varying the input chlorophyll concentration while keeping all other inputs constant. Black lines show the default COARE3.5 model's predictions of warm layer magnitude and depth for the 2019 research cruise onboard R/V Falkor. Colored lines show the differences from the

black lines when the COARE3.5 model is run with the new parameterization at a variety of realistic chlorophyll concentrations.

6 Conclusion

We have developed the first radiant heating parameterization to offer both chlorophyll dependence and accuracy in the upper meter of the ocean while maintaining a computational simplicity reasonably comparable to its predecessors. Because it explicitly calculates the profile of photosynthetically available radiation (visible light), it can be used in biological and coupled bio-physical modeling as well. Using the new parameterization, we demonstrate the extent to which chlorophyll concentration can affect the depth and magnitude of DWLs, providing mechanistic insight into the possible interactions between phytoplankton and atmospheric convection. Moving forwards, we expect the parameterization – and the discussion of historical inaccuracies provided herein – to enable a needed step forward in accurate bio-physical modeling of upper ocean stratification, dynamics, and mixed-layer depths. We suggest the use of this parameterization in all future multi-level ocean modeling.

Acknowledgments

This research was funded by the National Science Foundation Award Number OCE 20-49546 and Schmidt Ocean Institute Contract Number CU19-1778 and CU19-3241. A.S. was supported by NASA grant 80NSSC21K0439 and by funding from the G. Unger Vetlesen Foundation and a fellowship from Columbia University's Center for Climate and Life. The authors would also like to thank the captains, officers, and crew of R/V Endeavour, R/V Meteor, and R/V Falkor.

Open Research

Data used in this study (Witte et al., 2024) is archived for public access on Columbia Academic Commons (https://doi.org/10.7916/wmdm-vm51). The code used to produce the figures in this study is available for public access on Github (https://github.com/Zappa-Lab/Bio-Physical-Radiant-Heating-Parameterization).

References

Bannehr, L., & Glover, V. (1991). Preprocessing of airborne pyranometer data. *NCAR Technical Note*, 45.

Bellenger, H., & Duvel, J.-P. (2009). An Analysis of Tropical Ocean Diurnal Warm Layers. *Journal of Climate*, *22*(13), 3629–3646. https://doi.org/10.1175/2008JCLI2598.1

Blackburn, W. J., & Proctor, J. T. A. (1983). Estimating photosynthetically active radiation from measured solar irradiance. *Sol. Energy; (United Kingdom)*, *31:2*. https://www.osti.gov/etdeweb/biblio/5060541

Britton, C. M., & Dodd, J. D. (1976). Relationships of photosynthetically active radiation and shortwave irradiance. *Agricultural Meteorology*, *17*(1), 1–7. https://doi.org/10.1016/0002-1571(76)90080-7

Defant, A. (1961). Physical oceanography. *(No Title)*. https://cir.nii.ac.jp/crid/1130282271105191040

Denman, K. L. (1973). A Time-Dependent Model of the Upper Ocean. *Journal of Physical Oceanography*, *3*(2), 173–184. https://doi.org/10.1175/1520-0485(1973)003<0173:ATDMOT>2.0.CO;2

Dickey, T. D., & Simpson, J. J. (1983). The influence of optical water type on the diurnal response of the upper ocean. *Tellus B*, *35B*(2), 142–154. https://doi.org/10.1111/j.1600-0889.1983.tb00018.x

Diffey, B. (2015). Solar Spectral Irradiance and Summary Outputs Using Excel. *Photochemistry and Photobiology*, *91*(3), 553–557. https://doi.org/10.1111/php.12422

Fairall, C. W., Bradley, E. F., Godfrey, J. S., Wick, G. A., Edson, J. B., & Young, G. S. (1996). Cool-skin and warm-layer effects on sea surface temperature. *Journal of Geophysical Research: Oceans*, *101*(C1), 1295–1308. https://doi.org/10.1029/95JC03190

Fairall, C. W., Bradley, E. F., Rogers, D. P., Edson, J. B., & Young, G. S. (1996). Bulk parameterization of air-sea fluxes for Tropical Ocean-Global Atmosphere Coupled-Ocean Atmosphere Response Experiment. *Journal of Geophysical Research: Oceans*, *101*(C2), 3747–3764. https://doi.org/10.1029/95JC03205

Frouin, R., Lingner, D. W., Gautier, C., Baker, K. S., & Smith, R. C. (1989). A simple analytical formula to compute clear sky total and photosynthetically available solar irradiance at the ocean surface. *Journal of Geophysical Research: Oceans*, *94*(C7), 9731–9742. https://doi.org/10.1029/JC094iC07p09731

Gentemann, C. L., Minnett, P. J., & Ward, B. (2009). Profiles of ocean surface heating (POSH): A new model of upper ocean diurnal warming. *Journal of Geophysical Research: Oceans*, *114*(C7). https://doi.org/10.1029/2008JC004825

Gildor, H., Sobel, A. H., Cane, M. A., & Sambrotto, R. N. (2003). A role for ocean biota in tropical intraseasonal atmospheric variability. *Geophysical Research Letters*, *30*(9). https://doi.org/10.1029/2002GL016759

Gnanadesikan, A., & Anderson, W. G. (2009). Ocean Water Clarity and the Ocean General Circulation in a Coupled Climate Model. *Journal of Physical Oceanography*, *39*(2), 314–332. https://doi.org/10.1175/2008JPO3935.1

Gnanadesikan, A., Emanuel, K., Vecchi, G. A., Anderson, W. G., & Hallberg, R. (2010). How ocean color can steer Pacific tropical cyclones. *Geophysical Research Letters*, *37*(18). https://doi.org/10.1029/2010GL044514

Goldberg, B., & Klein, W. H. (1977). Variations in the spectral distribution of daylight at various geographical locations on the earth's surface. *Solar Energy*, *19*(1), 3–13. https://doi.org/10.1016/0038-092X(77)90083-4

Hill, V. J. (2008). Impacts of chromophoric dissolved organic material on surface ocean heating in the Chukchi Sea. *Journal of Geophysical Research: Oceans*, *113*(C7). https://doi.org/10.1029/2007JC004119

Holmes, R. M., Zika, J. D., & England, M. H. (2019). Diathermal Heat Transport in a Global Ocean Model. *Journal of Physical Oceanography*, *49*(1), 141–161. https://doi.org/10.1175/JPO-D-18-0098.1

Howell, T. A., Meek, D. W., & Hatfield, J. L. (1983). Relationship of photosynthetically active radiation to shortwave radiation in the San Joaquin Valley. *Agricultural Meteorology*, *28*(2), 157–175. https://doi.org/10.1016/0002-1571(83)90005-5

Iudicone, D., Madec, G., & McDougall, T. J. (2008). Water-Mass Transformations in a Neutral Density Framework and the Key Role of Light Penetration. *Journal of Physical Oceanography*, *38*(7), 1357–1376. https://doi.org/10.1175/2007JPO3464.1

Ivanoff, A. (1977). Oceanic absorption of solar energy. *Modelling and Prediction of the Upper Layers of the Ocean*, 47–71.

Jerlov, N. G. (1968). *Optical oceanography*. Elsevier Pub. Co.

Jerlov, N. G. (1976). *Marine optics*. Elsevier Scientific Pub. Co.

Jin, D., Waliser, D. E., Jones, C., & Murtugudde, R. (2013). Modulation of tropical ocean surface chlorophyll by the Madden–Julian Oscillation. *Climate Dynamics*, *40*(1–2), 39–58. https://doi.org/10.1007/s00382-012-1321-4

Jochum, M., Yeager, S., Lindsay, K., Moore, K., & Murtugudde, R. (2010). Quantification of the Feedback between Phytoplankton and ENSO in the Community Climate System Model. *Journal of Climate*, *23*(11), 2916–2925. https://doi.org/10.1175/2010JCLI3254.1

Kahru, M., Leppanen, J.-M., & Rud, O. (1993). Cyanobacterial blooms cause heating of the sea surface. *Marine Ecology Progress Series*, *101*(1/2), 1–7.

Kantha, L. H., & Clayson, C. A. (1994). An improved mixed layer model for geophysical applications. *Journal of Geophysical Research: Oceans*, *99*(C12), 25235–25266. https://doi.org/10.1029/94JC02257

552 Katsaros, K. B., McMurdie, L. A., Lind, R. J., & DeVault, J. E. (1985). Albedo of a water surface, spectral variation,
553 effects of atmospheric transmittance, sun angle and wind speed. *Journal of Geophysical Research: Oceans*,
554 *90*(C4), 7313–7321. https://doi.org/10.1029/JC090iC04p07313
555 Kim, G. E., Pradal, M.-A., & Gnanadesikan, A. (2015). Quantifying the biological impact of surface ocean light
556 attenuation by colored detrital matter in an ESM using a new optical parameterization. *Biogeosciences*,
557 *12*(16), 5119–5132. https://doi.org/10.5194/bg-12-5119-2015
558 Kirk, J. T. O. (1994). *Light and Photosynthesis in Aquatic Ecosystems* (2nd ed.). Cambridge University Press.
559 https://doi.org/10.1017/CBO9780511623370
560 Kiss, A. E., Hogg, A. M., Hannah, N., Boeira Dias, F., Brassington, G. B., Chamberlain, M. A., Chapman, C.,
561 Dobrohotoff, P., Domingues, C. M., Duran, E. R., England, M. H., Fiedler, R., Griffies, S. M., Heerdegen,
562 A., Heil, P., Holmes, R. M., Klocker, A., Marsland, S. J., Morrison, A. K., … Zhang, X. (2020). ACCESS-
563 OM2 v1.0: A global ocean–sea ice model at three resolutions. *Geoscientific Model Development*, *13*(2),
564 401–442. https://doi.org/10.5194/gmd-13-401-2020
565 Kraus, E. B. (1972). *Atmosphere-Ocean Interaction. Clarendon*. Oxford.
566 Kvifte, G., Hegg, K., & Hansen, V. (1983). Spectral Distribution of Solar Radiation in the Nordic Countries. *Journal*
567 *of Applied Meteorology and Climatology*, *22*(1), 143–152. https://doi.org/10.1175/1520-
568 0450(1983)022<0143:SDOSRI>2.0.CO;2
569 Lee, Z., Du, K., Arnone, R., Liew, S., & Penta, B. (2005). Penetration of solar radiation in the upper ocean: A
570 numerical model for oceanic and coastal waters. *Journal of Geophysical Research: Oceans*, *110*(C9).
571 https://doi.org/10.1029/2004JC002780
572 Lee, Z., Wei, J., Voss, K., Lewis, M., Bricaud, A., & Huot, Y. (2015). Hyperspectral absorption coefficient of
573 "pure" seawater in the range of 350–550 nm inverted from remote sensing reflectance. *Applied Optics*,
574 *54*(3), 546–558. https://doi.org/10.1364/AO.54.000546
575 Lengaigne, M., Menkes, C., Aumont, O., Gorgues, T., Bopp, L., André, J.-M., & Madec, G. (2007). Influence of the
576 oceanic biology on the tropical Pacific climate in a coupled general circulation model. *Climate Dynamics*,
577 *28*(5), 503–516. https://doi.org/10.1007/s00382-006-0200-2
578 Lim, H.-G., Kug, J.-S., & Park, J.-Y. (2019). Biogeophysical feedback of phytoplankton on Arctic climate. Part II:
579 Arctic warming amplified by interactive chlorophyll under greenhouse warming. *Climate Dynamics*, *53*(5),
580 3167–3180. https://doi.org/10.1007/s00382-019-04693-5
581 Liu, T., Lee, Z., Shang, S., Xiu, P., Chai, F., & Jiang, M. (2020). Impact of Transmission Scheme of Visible Solar
582 Radiation on Temperature and Mixing in the Upper Water Column With Inputs for Transmission Derived
583 From Ocean Color Remote Sensing. *Journal of Geophysical Research: Oceans*, *125*(7), e2020JC016080.
584 https://doi.org/10.1029/2020JC016080
585 Manizza, M., Le Quéré, C., Watson, A. J., & Buitenhuis, E. T. (2005). Bio-optical feedbacks among phytoplankton,
586 upper ocean physics and sea-ice in a global model. *Geophysical Research Letters*, *32*(5).
587 https://doi.org/10.1029/2004GL020778
588 Marzeion, B., Timmermann, A., Murtugudde, R., & Jin, F.-F. (2005). Biophysical Feedbacks in the Tropical Pacific.
589 *Journal of Climate*, *18*(1), 58–70. https://doi.org/10.1175/JCLI3261.1
590 Mason, J. D., Cone, M. T., & Fry, E. S. (2016). Ultraviolet (250–550 nm) absorption spectrum of pure water.
591 *Applied Optics*, *55*(25), 7163–7172. https://doi.org/10.1364/AO.55.007163
592 McCree, K. J. (1966). A solarimeter for measuring photosynthetically active radiation. *Agricultural Meteorology*,
593 *3*(5), 353–366. https://doi.org/10.1016/0002-1571(66)90017-3
594 Mobley, C. D. (1994). *Light and water: Radiative transfer in natural waters*.
595 https://cir.nii.ac.jp/crid/1130282269840486656
596 Moeller, H. V., Laufkötter, C., Sweeney, E. M., & Johnson, M. D. (2019). Light-dependent grazing can drive
597 formation and deepening of deep chlorophyll maxima. *Nature Communications*, *10*(1), Article 1.
598 https://doi.org/10.1038/s41467-019-09591-2
599 Moon, P. (1940). Proposed standard solar-radiation curves for engineering use. *Journal of the Franklin Institute*,
600 *230*(5), 583–617. https://doi.org/10.1016/S0016-0032(40)90364-7

Morel, A. (1988). Optical modeling of the upper ocean in relation to its biogenous matter content (case I waters). *Journal of Geophysical Research: Oceans*, *93*(C9), 10749–10768. https://doi.org/10.1029/JC093iC09p10749

Morel, A., & Antoine, D. (1994). Heating Rate within the Upper Ocean in Relation to its Bio–optical State. *Journal of Physical Oceanography*, *24*(7), 1652–1665. https://doi.org/10.1175/1520-0485(1994)024<1652:HRWTUO>2.0.CO;2

Morel, A., Huot, Y., Gentili, B., Werdell, P. J., Hooker, S. B., & Franz, B. A. (2007). Examining the consistency of products derived from various ocean color sensors in open ocean (Case 1) waters in the perspective of a multi-sensor approach. *Remote Sensing of Environment*, *111*(1), 69–88. https://doi.org/10.1016/j.rse.2007.03.012

Morel, A., & Maritorena, S. (2001). Bio-optical properties of oceanic waters: A reappraisal. *Journal of Geophysical Research: Oceans*, *106*(C4), 7163–7180. https://doi.org/10.1029/2000JC000319

Murtugudde, R., Beauchamp, J., McClain, C. R., Lewis, M., & Busalacchi, A. J. (2002). Effects of Penetrative Radiation on the Upper Tropical Ocean Circulation. *Journal of Climate*, *15*(5), 470–486. https://doi.org/10.1175/1520-0442(2002)015<0470:EOPROT>2.0.CO;2

Nann, S., & Riordan, C. (1991). Solar Spectral Irradiance under Clear and Cloudy Skies: Measurements and a Semiempirical Model. *Journal of Applied Meteorology and Climatology*, *30*(4), 447–462. https://doi.org/10.1175/1520-0450(1991)030<0447:SSIUCA>2.0.CO;2

Ohlmann, J. C. (2003). Ocean Radiant Heating in Climate Models. *Journal of Climate*, *16*(9), 1337–1351. https://doi.org/10.1175/1520-0442(2003)16<1337:ORHICM>2.0.CO;2

Ohlmann, J. C., & Siegel, D. A. (2000). Ocean Radiant Heating. Part II: Parameterizing Solar Radiation Transmission through the Upper Ocean. *Journal of Physical Oceanography*, *30*(8), 1849–1865. https://doi.org/10.1175/1520-0485(2000)030<1849:ORHPIP>2.0.CO;2

Ohlmann, J. C., Siegel, D. A., & Mobley, C. D. (2000). Ocean Radiant Heating. Part I: Optical Influences. *Journal of Physical Oceanography*, *30*(8), 1833–1848. https://doi.org/10.1175/1520-0485(2000)030<1833:ORHPIO>2.0.CO;2

Ohlmann, J. C., Siegel, D. A., & Washburn, L. (1998). Radiant heating of the western equatorial Pacific during TOGA-COARE. *Journal of Geophysical Research: Oceans*, *103*(C3), 5379–5395. https://doi.org/10.1029/97JC03422

Papaioannou, G., Papanikolaou, N., & Retalis, D. (1993). Relationships of photosynthetically active radiation and shortwave irradiance. *Theoretical and Applied Climatology*, *48*(1), 23–27. https://doi.org/10.1007/BF00864910

Paulson, C. A., & Simpson, J. J. (1977). Irradiance Measurements in the Upper Ocean. *Journal of Physical Oceanography*, *7*(6), 952–956. https://doi.org/10.1175/1520-0485(1977)007<0952:IMITUO>2.0.CO;2

Paulson, C. A., & Simpson, J. J. (1981). The temperature difference across the cool skin of the ocean. *Journal of Geophysical Research: Oceans*, *86*(C11), 11044–11054. https://doi.org/10.1029/JC086iC11p11044

Payne, R. E. (1972). Albedo of the Sea Surface. *Journal of Atmospheric Sciences*, *29*(5), 959–970. https://doi.org/10.1175/1520-0469(1972)029<0959:AOTSS>2.0.CO;2

Pope, R. M., & Fry, E. S. (1997). Absorption spectrum (380–700 nm) of pure water. II. Integrating cavity measurements. *Applied Optics*, *36*(33), 8710–8723. https://doi.org/10.1364/AO.36.008710

Price, J. F., Weller, R. A., & Pinkel, R. (1986). Diurnal cycling: Observations and models of the upper ocean response to diurnal heating, cooling, and wind mixing. *Journal of Geophysical Research*, *91*(C7), 8411. https://doi.org/10.1029/JC091iC07p08411

Prytherch, J., Farrar, J. T., & Weller, R. A. (2013). Moored surface buoy observations of the diurnal warm layer. *Journal of Geophysical Research: Oceans*, *118*(9), 4553–4569. https://doi.org/10.1002/jgrc.20360

Rao, C. R. N. (1984). Photosynthetically active components of global solar radiation: Measurements and model computations. *Archives for Meteorology, Geophysics, and Bioclimatology Series B*, *34*(4), 353–364. https://doi.org/10.1007/bf02269448

649 Reineman, B. D., Lenain, L., Statom, N. M., & Melville, W. K. (2013). Development and Testing of Instrumentation
650 for UAV-Based Flux Measurements within Terrestrial and Marine Atmospheric Boundary Layers. *Journal*
651 *of Atmospheric and Oceanic Technology*, *30*(7), 1295–1319. https://doi.org/10.1175/JTECH-D-12-00176.1
652 Ricchiazzi, P., Yang, S., Gautier, C., & Sowle, D. (1998). SBDART: A Research and Teaching Software Tool for
653 Plane-Parallel Radiative Transfer in the Earth's Atmosphere. *Bulletin of the American Meteorological*
654 *Society*, *79*(10), 2101–2114. https://doi.org/10.1175/1520-0477(1998)079<2101:SARATS>2.0.CO;2
655 Rodskjer, N. (1983). Spectral daily insolation at Uppsala, Sweden. *Spectral Daily Insolation at Uppsala, Sweden*,
656 *33*(1–2), 89–98.
657 Sathyendranath, S., Gouveia, A. D., Shetye, S. R., Ravindran, P., & Platt, T. (1991). Biological control of surface
658 temperature in the Arabian Sea. *Nature*, *349*(6304), Article 6304. https://doi.org/10.1038/349054a0
659 Schmidt, W. (1908). Absorption der sonnenstrahlung im wasser. *SB Akad. Wiss. Wien*, *117*, 237–253.
660 Siegel, D. A., & Dickey, T. D. (1987). On the parameterization of irradiance for open ocean photoprocesses. *Journal*
661 *of Geophysical Research: Oceans*, *92*(C13), 14648–14662. https://doi.org/10.1029/JC092iC13p14648
662 Siegel, D. A., Ohlmann, J. C., Washburn, L., Bidigare, R. R., Nosse, C. T., Fields, E., & Zhou, Y. (1995). Solar
663 radiation, phytoplankton pigments and the radiant heating of the equatorial Pacific warm pool. *Journal of*
664 *Geophysical Research: Oceans*, *100*(C3), 4885–4891. https://doi.org/10.1029/94JC03128
665 Siegel, D. A., Westberry, T. K., & Ohlmann, J. C. (1999). Cloud Color and Ocean Radiant Heating. *Journal of*
666 *Climate*, *12*(4), 1101–1116. https://doi.org/10.1175/1520-0442(1999)012<1101:CCAORH>2.0.CO;2
667 Simpson, J. J., & Dickey, T. D. (1981). The Relationship between Downward Irradiance and Upper Ocean Structure.
668 *Journal of Physical Oceanography*, *11*(3), 309–323. https://doi.org/10.1175/1520-
669 0485(1981)011<0309:TRBDIA>2.0.CO;2
670 Smith, R. C., & Baker, K. S. (1978). Optical classification of natural waters 1: Optical classification. *Limnology and*
671 *Oceanography*, *23*(2), 260–267. https://doi.org/10.4319/lo.1978.23.2.0260
672 Smith, R. C., & Baker, K. S. (1981). Optical properties of the clearest natural waters (200–800 nm). *Applied Optics*,
673 *20*(2), 177–184. https://doi.org/10.1364/AO.20.000177
674 Soloviev, A. (1982). On the Vertical Structure of the Thin Surface Layer of the Ocean During a Weak Wind.
675 *Izvestiya, Atmospheric and Oceanic Physics*, *18*(7), 579–585.
676 Stock, C. A., Dunne, J. P., Fan, S., Ginoux, P., John, J., Krasting, J. P., Laufkötter, C., Paulot, F., & Zadeh, N.
677 (2020). Ocean Biogeochemistry in GFDL's Earth System Model 4.1 and Its Response to Increasing
678 Atmospheric CO2. *Journal of Advances in Modeling Earth Systems*, *12*(10), e2019MS002043.
679 https://doi.org/10.1029/2019MS002043
680 Strutton, P. G., & Chavez, F. P. (2004). Biological Heating in the Equatorial Pacific: Observed Variability and
681 Potential for Real-Time Calculation. *Journal of Climate*, *17*(5), 1097–1109. https://doi.org/10.1175/1520-
682 0442(2004)017<1097:BHITEP>2.0.CO;2
683 Sweeney, C., Gnanadesikan, A., Griffies, S. M., Harrison, M. J., Rosati, A. J., & Samuels, B. L. (2005). Impacts of
684 Shortwave Penetration Depth on Large-Scale Ocean Circulation and Heat Transport. *Journal of Physical*
685 *Oceanography*, *35*(6), 1103–1119. https://doi.org/10.1175/JPO2740.1
686 Tanre, D., Herman, M., Deschamps, P. Y., & Leffe, A. de. (1979). Atmospheric modeling for space measurements
687 of ground reflectances, including bidirectional properties. *Applied Optics*, *18*(21), 3587–3594.
688 https://doi.org/10.1364/AO.18.003587
689 Twelves, A. G., Goldberg, D. N., Henley, S. F., Mazloff, M. R., & Jones, D. C. (2021). Self-Shading and Meltwater
690 Spreading Control the Transition From Light to Iron Limitation in an Antarctic Coastal Polynya. *Journal of*
691 *Geophysical Research: Oceans*, *126*(2), e2020JC016636. https://doi.org/10.1029/2020JC016636
692 Weiss, A., & Norman, J. M. (1985). Partitioning solar radiation into direct and diffuse, visible and near-infrared
693 components. *Agricultural and Forest Meteorology*, *34*(2), 205–213. https://doi.org/10.1016/0168-
694 1923(85)90020-6
695 Wetzel, P., Maier-Reimer, E., Botzet, M., Jungclaus, J., Keenlyside, N., & Latif, M. (2006). Effects of Ocean
696 Biology on the Penetrative Radiation in a Coupled Climate Model. *Journal of Climate*, *19*(16), 3973–3987.
697 https://doi.org/10.1175/JCLI3828.1

Wick, G. A., Ohlmann, J. C., Fairall, C. W., & Jessup, A. T. (2005). Improved Oceanic Cool-Skin Corrections Using a Refined Solar Penetration Model. *Journal of Physical Oceanography*, *35*(11), 1986–1996. https://doi.org/10.1175/JPO2803.1

Witte, C. R., Zappa, C. J., & Subramaniam, A. S. (2024). Data For: An Improved Bio-Physical Parameterization for Radiant Heating in the Surface Ocean [Dataset]. Columbia Academic Commons. https://doi.org/10.7916/wmdm-vm51

Wu, T., Yu, R., Lu, Y., Jie, W., Fang, Y., Zhang, J., Zhang, L., Xin, X., Li, L., Wang, Z., Liu, Y., Zhang, F., Wu, F., Chu, M., Li, J., Li, W., Zhang, Y., Shi, X., Zhou, W., … Hu, A. (2021). BCC-CSM2-HR: A high-resolution version of the Beijing Climate Center Climate System Model. *Geoscientific Model Development*, *14*(5), 2977–3006. https://doi.org/10.5194/gmd-14-2977-2021

Yocum, C. S., Allen, L. H., & Lemon, E. R. (1964). Photosynthesis Under Field Conditions. VI. Solar Radiation Balance and Photosynthetic Efficiency1. *Agronomy Journal*, *56*(3), 249–253. https://doi.org/10.2134/agronj1964.00021962005600030001x

Zaneveld, J. R. V., Kitchen, J. C., & Pak, H. (1981). The influence of optical water type on the heating rate of a constant depth mixed layer. *Journal of Geophysical Research: Oceans*, *86*(C7), 6426–6428. https://doi.org/10.1029/JC086iC07p06426

Zaneveld, J. R. V., & Spinrad, R. W. (1980). An arc tangent model of irradiance in the sea. *Journal of Geophysical Research: Oceans*, *85*(C9), 4919–4922. https://doi.org/10.1029/JC085iC09p04919

Zhang, X., Hu, L., & He, M.-X. (2009). Scattering by pure seawater: Effect of salinity. *Optics Express*, *17*(7), 5698–5710. https://doi.org/10.1364/OE.17.005698